Plasma Physics, Vol. 16, pp. 565 to 587. Pergamon Press 1974. Printed in Northern Ireland

# AMPLIFICATION AND ABSORPTION OF ELECTROMAGNETIC WAVES IN OVERDENSE PLASMAS*

R. B. WHITE
Institute for Advanced Study, Princeton, N.J. 08540, U.S.A.
and
F. F. CHEN
University of California, Los Angeles, Ca. 90024, U.S.A.

(*Received* 24 *September* 1973; *and in final form* 13 *November* 1973)

**Abstract**—The spatial variation of the amplitude of electromagnetic radiation propagating into an inhomogeneous plasma is discussed in reference to nonlinear interaction of HCN laser radiation with plasmas and to experiments on r.f. heating of the ionosphere. Previous results on the ordinary wave and on the extraordinary wave at normal incidence are reviewed with emphasis on the physical processes affecting the amplitude behaviour. New numerical results are obtained starting from an integral representation of the solution of the wave equation for waves in a cold, inhomogeneous, magnetized plasma slab. Resonance absorption is discussed for the cases of normal incidence in the presence of a magnetic field (the Budden problem) and oblique incidence in the absence of a magnetic field.

## 1. INTRODUCTION

RECENT developments in laser technology make possible the exploration of the electromagnetic spectrum in the wavelength range between 10 and 1000 $\mu$m (1 mm). The most powerful lasers in this range are the $CO_2$ laser at 10·6 $\mu$m and the HCN laser at 337 $\mu$m. By using plasmas in the density range $n = 10^{15}$–$n = 10^{19}$ cm$^{-3}$ as targets, the study of nonlinear optics can be made more precise than in solid targets, since the nonlinear matrix elements can be calculated from classical electromagnetics.

The amplitude of a wave in a magnetized plasma, however, undergoes large spatial variations because of zeroes and infinities in the index of refraction. The approximation of geometrical optics is not useful in such cases; the wave form must be calculated by more exact methods before the wave amplitude can be inserted into any nonlinear theory. The gradient of the amplitude is also important, since this is proportional to the local radiation pressure, which can cause a low-frequency motion of the ions (HORA, 1969; LINDL and KAW, 1971).

In Section 2, we discuss the propagation of electromagnetic radiation in an inhomogeneous medium, analyzing cutoff and resonance points for several cases of practical interest. In Section 3 the linear absorption of radiation at a resonance point is analyzed.

Our results are also relevant to the problems of double-resonance coupling of microwaves to low-frequency waves (WONG *et al.*, 1970, 1971) and of r.f. heating of the ionosphere by the mechanism of parametric instabilities. Indeed, the subject of this paper has been treated extensively in connection with ionospheric radio propagation. Actual numerical computations, however, are rarely available.

## 2. PENETRATION OF A PLASMA BY ELECTROMAGNETIC WAVES

### 2.1 *Fundamental equations*

Consider a plane electromagnetic wave $\mathbf{E} = \mathbf{E}_0 \exp i(\mathbf{k}\cdot\mathbf{r} - \omega t)$ propagating into a static plasma with a uniform magnetic field $\mathbf{B}_0$ in the $z$ direction and density gradient

* Work supported by the U.S. Atomic Energy Commission, Contract AT(04-3)-34, Project 157.

$\nabla n_0$ in the $x$ direction. From Maxwell's equations (e.s.u.)

$$\nabla \times \mathbf{E} = i\omega \mathbf{B} \tag{1}$$

$$c^2 \nabla \times \mathbf{B} = -4\pi n_0 e \mathbf{v} - i\omega \mathbf{E}, \tag{2}$$

one obtains the linear wave equation

$$\nabla(\nabla \cdot \mathbf{E}) - \nabla^2 \mathbf{E} - \frac{\omega^2}{c^2}\mathbf{E} = -\frac{4\pi i \omega e n_0(x)}{c^2}\mathbf{v}, \tag{3}$$

where ion motions have been neglected, and the electron velocity $\mathbf{v}$ is given by

$$\frac{\partial \mathbf{v}}{\partial t} = -\frac{e}{m}(\mathbf{E} + \mathbf{v} \times \mathbf{B}_0) - \nu \mathbf{v}. \tag{4}$$

For zero collision frequency $\nu$, equation (3) can be written as follows:

$$(k_y^2 + k_z^2 - k_0^2 + \kappa^2)E_x + ik_y \frac{\partial E_y}{\partial x} + ik_z \frac{\partial E_z}{\partial x} - \frac{i\omega_c}{\omega}\kappa^2 E_y = 0 \tag{5}$$

$$ik_y \frac{\partial E_x}{\partial x} + \frac{i\omega_c}{\omega}\kappa^2 E_x - \frac{\partial^2 E_y}{\partial x^2} + (k_z^2 - k_0^2 + \kappa^2)E_y - k_y k_z E_z = 0 \tag{6}$$

$$ik_z \frac{\partial E_x}{\partial x} - k_y k_z E_y - \frac{\partial^2 E_z}{\partial x^2} + \left(k_y^2 - k_0^2 + \frac{\omega_p^2}{c^2}\right)E_z = 0, \tag{7}$$

where $k_0 \equiv \omega/c$ and

$$\kappa^2(x) \equiv k_0^2 \frac{\omega_p^2}{\omega^2 - \omega_c^2}, \tag{8}$$

$\omega_p^2$ and $\omega_c$ being $4\pi n_0(x)e^2/m$ and $eB_0/m$ respectively. The fact that $k_y$ and $k_z$ are not functions of $x$ is a consequence of Snell's Law (GINZBURG, 1964*a*), the index of refraction varying only in the $x$ direction in this case.

(a) *Normal incidence*, $k_y = k_z = 0$. In this case equation (7) is decoupled from equations (5) and (6):

$$\frac{\partial^2 E_z}{\partial x^2} + k_0^2\left(1 - \frac{\omega_p^2}{\omega^2}\right)E_z = 0. \tag{9}$$

This is the wave equation for the *ordinary mode*, whose well known solution is given in Section 3. Equations (5) and (6) become

$$\frac{\partial^2 E_y}{\partial x^2} + k_0^2\left(1 - \frac{\omega_p^2}{\omega^2}\frac{\omega^2 - \omega_p^2}{\omega^2 - \omega_h^2}\right)E_y = 0 \tag{10}$$

$$\frac{iE_x}{E_y} = \frac{\omega_c}{\omega}\frac{\omega_p^2(x)}{\omega^2 - \omega_h^2(x)}, \tag{11}$$

where $\omega_h$ is the upper hybrid frequency: $\omega_h^2 = \omega_p^2 + \omega_c^2$. The bracket in equation (10) will be recognized as the dielectric constant for the *extraordinary mode* in a uniform plasma. Equation (10) will be discussed in Section 2.3.

(b) *Oblique incidence*, $k_z = 0$. If the wave enters the plasma obliquely *in the plane perpendicular to* $B_0$, equations (5)–(7) become

$$(k_y^2 - k_0^2 + \kappa^2)E_x + ik_y \frac{\partial E_y}{\partial x} - \frac{i\omega_c}{\omega}\kappa^2 E_y = 0 \tag{12}$$

$$ik_y \frac{\partial E_x}{\partial x} + \frac{i\omega_c}{\omega}\kappa^2 E_x - \frac{\partial^2 E_y}{\partial x^2} + (\kappa^2 - k_0^2)E_y = 0 \tag{13}$$

$$\frac{\partial^2 E_z}{\partial x^2} + k_0^2\left(1 - \frac{\omega_p^2}{\omega^2} - \frac{k_y^2}{k_0^2}\right)E_z = 0. \tag{14}$$

The ordinary and extraordinary modes are still separable. Equation (14) for the ordinary mode has been treated previously and will be discussed in Section 2.2.

(c) *Oblique incidence*, $k_y = 0$. If the wave is incident obliquely *with a component of* $\mathbf{k}$ *along* $\mathbf{B}_0$, equations (5)–(7) are no longer separable into ordinary and extraordinary modes, and a fourth-order differential equation must be solved for the wave amplitude variation. The normal modes are then given by the Appleton–Hartree dispersion relation, and the fluid case has been discussed in the standard texts (BUDDEN, 1961; GINZBURG, 1964). Moreover, the finiteness of $k_z$ means that Landau damping has to be taken into account via the Vlasov equation. This problem has been analyzed by PEARLSTEIN and BHADRA (1969) but is not of interest here because no new effects of wave amplification occur if $k_z \neq 0$.

## 2.2 *The ordinary mode*

(a) *Perpendicular incidence.* The geometry for this case is illustrated in Fig. 1. Since **E** lies entirely along $\mathbf{B}_0$, there is in the linear theory no cyclotron motion of the

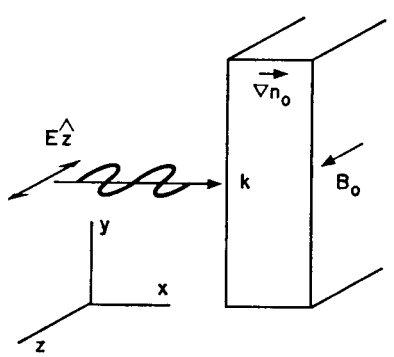


FIG. 1.—Geometry for the ordinary wave, TE mode.

electrons; and the wave equation, equation (9), is the same as for an unmagnetized plasma. The solution of equation (9) can be expressed in terms of well-known functions if the density and, hence, the index of refraction

$$\varepsilon(x) = 1 - \frac{\omega_p^2(x)}{\omega^2} \tag{15}$$

is a simple function of $x$. If $n_0(x)$ is linear and $\varepsilon = 1 - (x/x_0)$ (Fig. 2), a simple

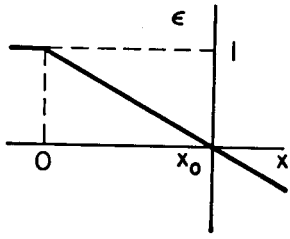


FIG. 2.—Linear behavior of the dielectric constant which gives rise to Airy function solutions.

substitution (BREKHOVSKIKH, 1960; BUDDEN, 1961*a*; GINZBURG, 1964*a*) brings equation (3) into the form

$$\frac{\mathrm{d}^2E}{\mathrm{d}\zeta^2} + \zeta E = 0, \tag{16}$$

where $\zeta \equiv (k_0^2/x_0)^{1/3}\,(x_0 - x)$. The solution of equation (16) can be given in terms of Bessel functions of order $\frac{1}{3}$ or as an Airy function:

$$E(\zeta) = \frac{3}{\pi} A \int_0^\infty \cos\left(\tfrac{1}{3}x^3 - \zeta x\right) \mathrm{d}x \propto Ai(-\zeta). \tag{17}$$

This solution is shown in Fig. 3 for $k_0x_0 = 5$, corresponding to a typical laboratory

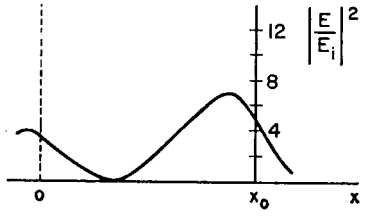


FIG. 3.—Wave intensity distribution for linear density profile, $k_0x_0 = 5$.

experiment, and in Fig. 4 for $k_0x_0 = 70$, corresponding to an ionospheric or fusion-oriented experiment. These two curves are, of course, simply different scalings of the same function of $\zeta$.

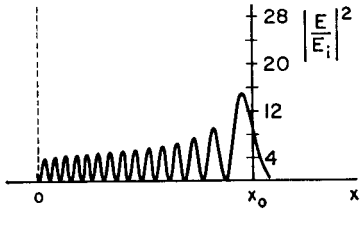


FIG. 4.—Wave intensity distribution for linear density profile, $k_0x_0 = 70$.

The amplification factor is easily found as follows. The electric field amplitude $|E|$ reaches a maximum $|E_m|$ several free-space wavelengths in front of the cutoff layer; $|E_m/A|^2$ has a value of 2·68. The distance between the plasma boundary and the cutoff layer (see Fig. 2) is

$$\zeta_0 = (k_0^2/x_0)^{1/3}x_0 = (k_0x_0)^{2/3}. \tag{18}$$

If $\zeta_0$ is sufficiently large, we may use the asymptotic expansion of equation (17) at the boundary:

$$E(\zeta_0) \approx \frac{3A}{\pi^{1/2}\zeta_0^{1/4}} \cos\left(\tfrac{2}{3}\zeta^{3/2} - \frac{\pi}{4}\right).$$

At a peak of the amplitude distribution near the boundary, we have

$$\left|\frac{E}{A}\right|^2 \approx \frac{9}{\pi}\zeta_0^{-1/2} = \frac{9}{\pi}(k_0x_0)^{-1/3}.$$

Since we have neglected dissipation, this peak results from the constructive interference of the incident wave with a reflective wave of the same amplitude. Hence, the incident wave has amplitude $|E_i/A|^2 = (9/4\pi)\,(k_0x_0)^{-1/3}$. Dividing 2·68 by this, we have the amplification factor

$$\left|\frac{E_m}{E_i}\right|^2 = 3{\cdot}74(k_0x_0)^{1/3}, \tag{19}$$

essentially the result given by GINZBURG (1964*b*). Here $x_0$ can be interpreted more generally as the density scale length

$$\Lambda \equiv \frac{n_c}{n_0'} = \left(\frac{4\pi e^2}{m\omega^2}\frac{\partial n_0}{\partial x}\right)^{-1}. \tag{20}$$

Because of the weak dependence on $k_0\Lambda$, the enhancement factor (19) varies only between 10 and 100 in a wide variety of applications. In laboratory experiments with microwaves, it is about 5; with lasers, about 15. In ionospheric experiments (WONG and TAYLOR, 1971) it can be as much as 80. For 337-$\mu$m radiation in a fusion plasma of 1 meter radius, the factor would be 100.

Equation (3) has also been solved analytically for other density profiles (BUDDEN, 1961b; GINZBURG, 1964a; BANOS and KELLY, 1972). Larger enhancement factors can be achieved if the density gradient decreases near the cutoff layer. For instance, Fig. 5 shows computations for a parabolic profile with $n_0'$ vanishing at the reflection

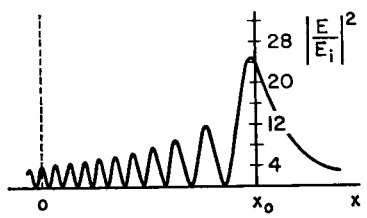


FIG. 5.—Wave intensity distribution for parabolic density profile, $k_0x_0 = 70$.

layer; i.e. for $\varepsilon = (1 - x/x_0)^2$. The amplification factor is 21·9, compared with 14·9 for the linear profile of Fig. 4, which has the same number of free-space wavelengths between the boundary and the critical layer. The physical reason for this dependence on profile is easy to see. If $n_0$ varies slowly in the region near the cutoff layer, where $\varepsilon$ is small, the last lobe of the amplitude pattern is greatly stretched out and hence can rise to a higher value before falling again to match the solution in the evanescent layer.

When collisions are taken into account, the enhancement factor given by equation

(19) may be largely illusory. Retaining the $\nu$ term in equation (4) yields the dielectric constant

$$\varepsilon = 1 - \frac{\omega_p^2}{\omega^2}\left(1 + \frac{i\nu}{\omega}\right)^{-1}. \tag{21}$$

For constant $\nu$, collisional attenuation of a wave as it traverses a linear density profile to the cutoff and back out again results in a reflection coefficient (BUDDEN, 1961a; GINZBURG, 1964a)

$$|R| = \exp\left(-\frac{4}{3}\frac{\nu}{\omega}k_0 x_0\right). \tag{22}$$

The effect of this on $|E_m|^2$ can be seen as follows. The intensity $E_1^2$ of the *incoming* wave at the principal maximum in the absence of collisions is given by $\frac{1}{4}$ of equation (19):

$$\left|\frac{E^1}{E_i}\right|^2 \approx 0{\cdot}9(k_0 x_0)^{1/3}.$$

When $\nu > 0$, $|E_1|$ is diminished by approximately a factor $|R|^{1/2}$, since half the losses represented by equation (22) occur in the reflected wave. When $E_1$ interferes constructively with the reflected wave, the intensity must again be multiplied by 4, resulting in

$$\left|\frac{E_m}{E_i}\right|^2 \approx 3{\cdot}7\,|R|\,(k_0 x_0)^{1/3}. \tag{23}$$

The coefficient in equation (23) is somewhat increased if the effect of $\nu$ on the Airy function solution is accurately taken into account (GINZBURG, 1964a).

For the ionosphere, GINZBURG (1964*a*) has already shown that collisions reduce the field enhancement factor from about 80 to the factor of 4 one would get from reflection from a simple mirror. For a laboratory arc plasma with $n_{av} = 5 \times 10^{15}\text{cm}^{-3}$, $T_e = 1{\cdot}5$ eV, and $x_0 = 0{\cdot}5$ cm, the ratio $\nu_{ei}/\omega$ is $6 \times 10^{-3}$ for 337-$\mu$ radiation (HEALD and WHARTON, 1965). Equations (22) and (23) then yield

$$|E_m/E_i|^2 \approx 7.5,$$

as compared with about 15 for $T_e = 5$ eV, and about 17 for a collisionless plasma. Under fusion conditions ($T_e > 10$ KeV), $|R|$ is essentially unity; and the factor 100 mentioned above is still valid. At the other extreme, in $Q$-machine experiments (WONG *et al.*, 1971) with 10-cm microwaves, in which $n = 10^{11}\,\text{cm}^{-3}$ and $T_e = 0{\cdot}22\,\text{eV}$, $\nu/\omega$ is $1{\cdot}3 \times 10^{-3}$; collisional attenuation is then negligible. Since $k_0 x_0 \approx 1$ in the experiments of WONG *et al.* (1971), equation (19) or (23) predicts only the factor of 4 enhancement given by a simple mirror reflection; in fact, with $\Lambda \ll \lambda$, finite-geometry effects would decrease this factor further. Double-resonance coupling using the ordinary mode, therefore, would not be expected to be highly localized.

(b) *Oblique incidence, TE mode.* Consider now the case of oblique incidence at an angle $\theta_0$ to the direction of $\nabla n_0$. In the absence of a magnetic field, the ordinary wave can be polarized with **E** in the plane of incidence or *perpendicular to it*, with markedly different results. In the *latter case*, which may be called the TE (transverse electric) mode, the geometry is as shown in Fig. 6. The electric field $\mathbf{E} = E_z\hat{z}$ obeys equation

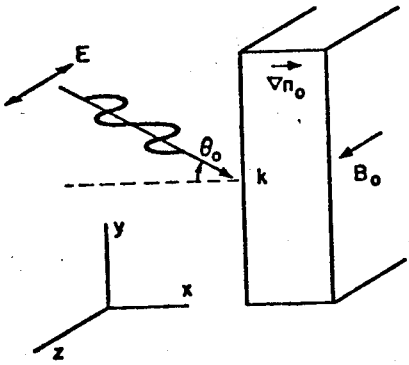


FIG. 6.—Geometry for the ordinary wave, TE mode.

(14). Since $k_y = k \sin\theta$ is constant by Snell's Law, it is equal to $k_0 \sin\theta_0$; and equation (14) can be written

$$\frac{\partial^2 E_z}{\partial x^2} + k_0^2\left(1 - \frac{\omega_p^2}{\omega^2} - \sin^2\theta_0\right)E_z = 0. \tag{24}$$

Alternatively, we may write equation (14) as

$$\frac{\partial^2 E_z}{\partial x^2} - k_y^2 E_z + k_0^2 \varepsilon E_z = 0, \tag{25}$$

where $\varepsilon$ denotes the ordinary-wave dielectric constant given by equation (15). The reason for the $k_y^2$ term is obvious from equation (25): since $\varepsilon$ is isotropic in the plane perpendicular to $\mathbf{B}_0$, the wave equation must become $\mathbf{E}'' + k_0^2 \varepsilon \mathbf{E} = 0$ in the limit of a uniform plasma. The $k_y^2$ term is needed because the $x$-axis was not chosen along $k$. Because of this term, the cutoff occurs at a lower value of $\omega_p$ than for perpendicular incidence, as seen from equation (24):

$$\omega_p = \omega \cos\theta_0. \tag{26}$$

For a linear density profile, one again obtains equation (16), where $\zeta$ is now defined as $\zeta \equiv (k_0^2/x_0)^{1/3}(x_0 \cos^2\theta_0 - x)$. The amplitude variation is as shown in Figs. 3 and 4, except that the cutoff now occurs at the point where

$$\varepsilon = \tilde{n}^2 = \sin^2\theta_0. \tag{27}$$

The wave is reflected earlier because of refraction in the outer layers of the plasma, and the enhancement factor is less than in the previous case.

(c) *Oblique incidence, TM mode.* If E is polarized to lie *in* the plane of incidence, as illustrated in Fig. 7, the wave is ordinary only if $\mathbf{B}_0 = 0$. Now it is the oscillating magnetic field which is transverse (to $\nabla n_0$). As pointed out by GINZBURG (1964*a*), the wave amplitude exhibits a fundamentally different behaviour in this case. The reason for this is shown in Fig. 8. As the electrons oscillate in the direction of E, a component of their motion lies along $\nabla n_0$ as long as $\theta_0 > 0$. This component

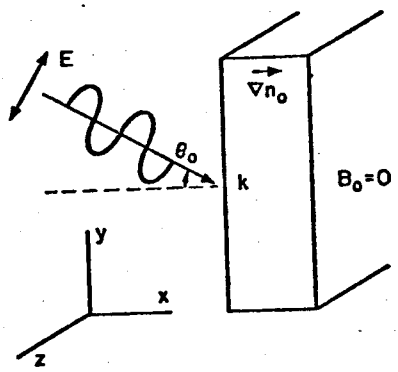


FIG. 7.—Geometry for the ordinary wave, TM mode.

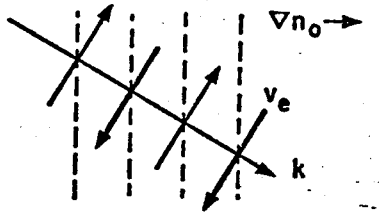


FIG. 8.—Motion of electrons in the ordinary wave, TM mode.

causes an electrostatic charge separation, and the wave cannot remain purely electromagnetic. Specifically, the electrostatic part of E can be obtained by taking the divergence of Maxwell's equation

$$c^2\nabla \times \mathbf{B} = -i\omega\varepsilon\mathbf{E}. \tag{28}$$

Thus

$$0 = \varepsilon\nabla\cdot\mathbf{E} + \mathbf{E}\cdot\nabla\varepsilon$$

$$\nabla\cdot\mathbf{E} = -\mathbf{E}\cdot\nabla(\ln\varepsilon). \tag{29}$$

This mode is described by equations (12) and (13) in the limit $\omega_c \to 0$; it is simpler, however, to use equations (12) and (29). With the help of equation (8), equation (12) now reads, for $\mathbf{B}_0 = 0$,

$$\left(k_y^2 - k_0^2 + \frac{\omega_p^2}{c^2}\right)E_x + ik_y\frac{\partial E_y}{\partial x} = 0. \tag{30}$$

Substituting for $E_y$ from equation (29) and using equation (15) for $\varepsilon$, we have

$$E_x'' + k_0^2(\varepsilon - \sin^2\theta_0)E_x + [E_x(\ln\varepsilon)']' = 0, \tag{31}$$

where the prime denotes $\partial/\partial x$. The first derivative can be removed by the transformation

$$E_x = G\sin\theta = G\sin\theta_0/\varepsilon^{1/2}, \tag{32}$$

which, for $\sin\theta_0 \neq 0$, brings equation (31) into the form

$$G'' + [k_0^2(\varepsilon - \sin^2\theta_0) + \tfrac{1}{2}(\ln\varepsilon)'' - \tfrac{1}{4}(\ln\varepsilon)'^2]G = 0. \tag{33}$$

The effective dielectric constant is, therefore,

$$\varepsilon_{eff} = \varepsilon - \sin^2\theta_0 + \left(\frac{\lambda_0}{2\pi}\right)^2\left(\frac{1}{2}\frac{\varepsilon''}{\varepsilon} - \frac{3}{4}\frac{\varepsilon'^2}{\varepsilon^2}\right). \tag{34}$$

If $\lambda_0$ is much smaller than the scale length of $\varepsilon$, the last two terms are negligible except near the layer where $\varepsilon \approx 0$. Consequently, the TM mode has a cutoff nearly at the same place as the TE mode does. The wave amplitude near cutoff has nearly the same behaviour as that prescribed by equation (24), except that it is $G = \sqrt{\varepsilon}\, E_x / \sin\theta_0$ rather than $E_x$ which satisfies this equation. When $\varepsilon$ is sufficiently small, however, $\varepsilon_{eff}$ becomes infinite. For $\varepsilon \propto -x^p$, equation (34) becomes

$$\varepsilon_{eff} = \varepsilon - \sin^2\theta_0 - \frac{1}{k_0^2 x^2}\frac{p}{2}\left(1 + \frac{p}{2}\right), \tag{35}$$

and $\varepsilon_{eff}$ diverges as $1/x^2$, as illustrated in Fig. 9.

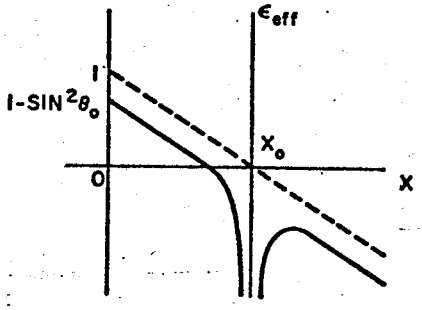


FIG. 9.—Schematic of the effective dielectric constant for the ordinary wave, TM mode.

The case of a linear profile, $p = 1$, has been treated extensively by DENISOV (1957) in connection with the ionosphere and by FREIDBERG *et al.* (1972) in connection with laser-fusion. In the neighbourhood of $\varepsilon = 0$, equations (33) and (35) give, for $p = 1$,

$$G'' \approx \frac{3}{4x^2} G, \tag{36}$$

so that $G \propto x^{-1/2}$, and $E_x \propto \sin\theta_0/x$. This behaviour, with the infinity removed by collisions, is shown in Fig. 10. Beyond the cutoff at the layer where $\varepsilon \approx \sin^2\theta_0$, the wave is exponentially attenuated. If the evanescence region is not too thick, the amplitude becomes large again at the resonance layer $\varepsilon = 0$. The physical reason for the infinity of $E$ here is, of course, that *$E$ has a frequency equal to the natural*

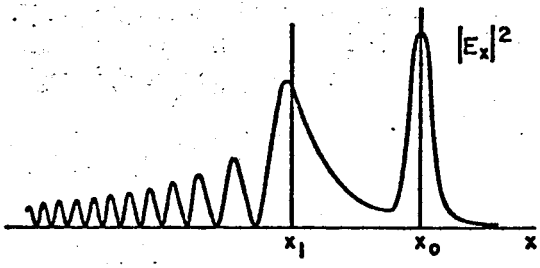


FIG. 10.—Schematic of the wave intensity distribution for the ordinary wave, TM mode.

*oscillation frequency* $\omega_p$ of the electrons, and plasma oscillations build up in amplitude to a value limited by collisions or nonlinear effects. The TM ordinary wave has the property that both components of $E$ become infinite at the resonance layer. $E_y$ can be found from equation (29); it behaves as log $x$ near $\varepsilon = 0$. The wave magnetic field, however, is finite at $\varepsilon = 0$; and it is clear that the infinity in $|E|$ is associated with its electrostatic component. Numerical computations of the various field quantities may be found in FREIDBERG *et al.* (1972).

The field enhancement factor at resonance will depend on the collision rate. From equation (21) and (32), we have, for $\omega_p = \omega_s$ and $p = 1$,

$$|E_{xm}| = \left| \frac{G \sin \theta_0}{\sqrt{i\nu/\omega}} \right| = \frac{R(\theta_0) \sin \theta_0}{\sqrt{\nu/\omega}}, \tag{37}$$

where $R(\theta_0)$ is the coefficient of $G$ at $\omega = \omega_p$. That is, $G = R(\theta_0)/x^{1/2} = R/(-\varepsilon)^{1/2}$ near $x = 0$. The behaviour of $|E_{xm}|$ at resonance was analyzed by DENISOV (1957)

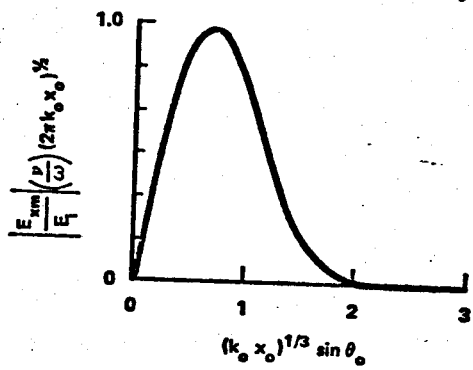


FIG. 11.—Amplification factor as a function of angle for the ordinary wave, TM mode (from Denisov).

with the result shown in Fig. 11. For small sin $\theta_0$, $|E_m/E_i|$ is small because the electron motion is almost parallel to surfaces of constant $n_0$, and the electrostatic charge separation is small. For large sin $\theta_0$, $|E_m/E_i|$ is small because the cutoff and resonance regions are widely separated, and the wave is greatly attenuated in the evanescence region. The angle of incidence $\theta_0$, therefore, can be adjusted for maximum amplification.

As a numerical example, consider the arc plasma discussed previously: $n_0 = 10^{16}$ cm$^{-3}$, $T_e = 1{\cdot}5$ eV, $k_0 x_0 = 93$, $\nu_{ei}/\omega = 1{\cdot}2 \times 10^{-2}$. Since the peak of the curve of Fig. 11 is around unity, we have $|E_{xm}/E_i|^2 \approx 12$, as compared with 7·5 for the intensity near cutoff. This result, however, is proportional to $\nu_{ei}^{-2} \approx T_e^3$. At $T_e = 5$ eV, we would have $|E_{xm}/E_i|^2 \approx 400$. Field amplification at resonance, therefore, can be much larger than at cutoff, even when the component $E_y$ is neglected. The optimum angle of incidence in this case is $\theta_0 = 8°$.

The half width of the curve of Fig. 11 gives $\Delta\theta_0 \approx \Delta \sin \theta_0 \approx (k_0 x_0)^{-1/3}$. In the present example, significant amplification is achieved between 3° and 16°. The angular range, however, becomes rather small for large plasmas, such as those encountered in fusion reactors or in space. For $k_0 x_0 = 10^4$, $\Delta\theta_0$ is only 2·7°; and extreme care must be taken in the collimation of the incident beam. In such plasmas the evanescence layer is thick compared with the wavelength unless $\theta_0$ is small;

hence the angular range in which appreciable tunneling of the radiation occurs is limited.

In addition to the enhancement of $|E|$ at resonance, there is an even greater enhancement of the radiation pressure gradient $\nabla E^2/8\pi$, leading to a ponderomotive force on the ions (HORA, 1969). The scale length of the resonance peak is given by the condition that the real part of $\varepsilon$ be comparable to the imaginary part; i.e. for a linear profile,

$$\frac{\Delta x}{x_0} \approx \frac{\nu}{\omega}. \tag{38}$$

The pressure-gradient scale-length, therefore, is shorter than the density scale-length by a factor $\nu/\omega$. A further effect at the resonance is the absorption of energy there, even in the absence of collisions. This mechanism will be discussed further in Section 3.

### 2.3 *The extraordinary wave at normal incidence (the Budden problem)*

For the geometry of Fig. 12, with $\mathbf{k} = k\hat{x}$ and E polarized perpendicular to $\mathbf{B}_0$, the appropriate equations are equations (10) and (11). Defining

$$\varepsilon_x \equiv 1 - \frac{\omega_p^2}{\omega^2}\frac{\omega^2 - \omega_p^2}{\omega^2 - \omega_h^2} = \frac{k^2(x)}{k_0^2}, \tag{39}$$

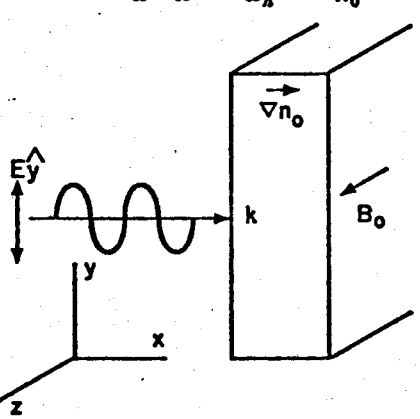


FIG. 12.—Geometry for the extraordinary wave, normal incidence.

we may write equation (10) as

$$\frac{d^2E_y}{dx^2} + k_0^2\varepsilon_x E_y = 0. \tag{40}$$

The behaviour of $\varepsilon_x$ is shown in Fig. 13.

As the wave propagates into regions of increasing $\omega_p$, it first encounters the right-hand cutoff ($\varepsilon_x = 0$) at

$$\frac{\omega_{p1}^2}{\omega^2} = 1 - \frac{\omega_c}{\omega}, \tag{41}$$

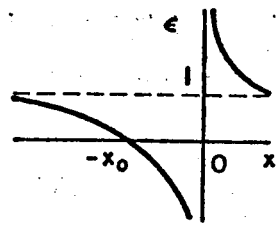


FIG. 13.—Behavior of the dielectric constant for the extraordinary wave, normal incidence.

and then the upper hybrid resonance ($\varepsilon_x = \infty$) at

$$\frac{\omega_{p2}^2}{\omega^2} = 1 - \frac{\omega_c^2}{\omega^2}. \tag{42}$$

We shall assume that the left-hand cutoff, described by equation (41) with the sign reversed, does not occur within the plasma. Just as in the case of the ordinary TM mode at oblique incidence, there is reflection at the cutoff, then a layer of evanescence and tunneling, and finally a resonance with the natural oscillation frequency of the electron fluid, $\omega = \omega_h$ in this case. Consequently, the field amplitude behaves qualitatively as in Fig. 10. For the extraordinary wave at $\theta_0 = 0$, however, the separation $\delta_x$ of the cutoff and resonance layers is fixed by the plasma parameters. Dividing equation (42) by equation (41), we have

$$\frac{\omega_{p2}^2}{\omega_{p1}^2} = 1 + \frac{\omega_c}{\omega} = \frac{n_2}{n_1} \approx 1 + \frac{\delta x}{\Lambda}, \tag{43}$$

where the density ratio $n_2/n_1$ is expressed in terms of the density scale length $\Lambda$. Therefore,

$$\delta x = \frac{\omega_c}{\omega}\Lambda. \tag{44}$$

If $\lambda \ll \Lambda$, the wave cannot tunnel through to the hybrid resonance unless $B_0$ is extremely weak; the layer of non-propagation—of thickness $\delta x$—between the cutoff and resonance layers would then be many wavelengths thick.

The physical mechanism for a peak in $|E|^2$ at resonance is again the development of an electrostatic component of $E$, which excites upper-hybrid oscillations limited in amplitude only by collisions or nonlinear effects. In this case, the Lorentz force causes electrons to move in the direction of $\nabla n_0$, and hence develop a component $E_x$, even though E is purely in the $y$ direction outside the plasma. The structure of $\varepsilon_x$ (equation 39) is considerably simpler than that of $\varepsilon_{\text{eff}}$ (equation 34) for the ordinary wave at oblique incidence. By choosing a suitable density profile, one can reduce equation (40) to Whittaker's equation and make use of the asymptotic properties of Whittaker functions. The absence of derivatives of $\omega_p$ in $\varepsilon_x$ allows one to solve easily for the corresponding density distribution.

BUDDEN's (1961*c*) analysis of this problem is well known. One replaces equation (39) with a simple function containing a zero and an infinity (Fig. 13):

$$\varepsilon_x = 1 + \frac{x_0}{x}. \tag{45}$$

With $s \equiv k_0 x$ and $s_0 \equiv k_0 x_0$, equation (40) becomes

$$\frac{d^2 E_y}{ds^2} + \left(1 + \frac{s_0}{s}\right) E_y = 0. \tag{46}$$

This has the solution (BUDDEN, 1961*c*) $E_y = W_{k,m}(\zeta)$, where $W_{k,m}$ is Wittaker's function, $\zeta \equiv 2is$, $k = -i/2$, and $m = \pm\frac{1}{2}$. Although the reflection and transmission coefficients have been found from this solution, the field amplitude behaviour has not previously been computed, there being no suitable series representations of $W_{k,m}$ valid in all regions for the case $m = \pm\frac{1}{2}$. We have, therefore, computed the amplitude distribution using an integral representation.

Before giving the details of this, we show that equation (45) represents a reasonable density profile. Setting equation (45) equal to equation (39) yields a quadratic equation for the density $\omega_p^2/\omega^2$, with $\omega_c^2/\omega^2$, as a parameter. The solution is shown in Fig. 14. The cutoff and resonance points occur on different parts of the density

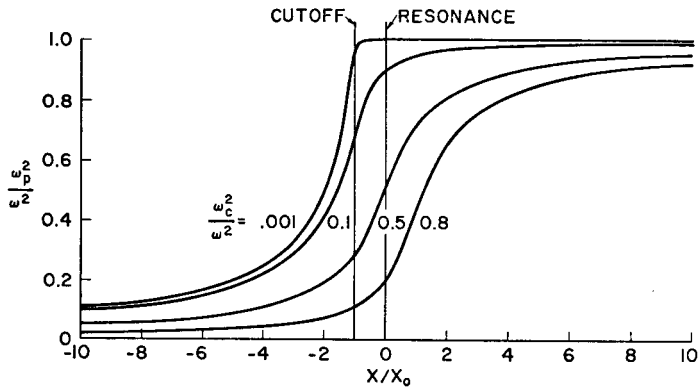


FIG. 14.—Density profiles corresponding to the assumed form of $\varepsilon(x)$ in the Budden problem.

profile depending on $\omega_c^2/\omega^2$, but in each case the density is a smoothly increasing function of $x$. An integral solution (WHITTAKER and WATSON, 1952; BANOS, 1972; WEYL, 1970; BERK and PEARLSTEIN, 1972) of equation (46) is

$$E_y(s) = Ase^{is} \int \exp -i\left(2ws - \tfrac{1}{2}s_0 \ln \frac{w-1}{w}\right) dw. \tag{47}$$

For finite $E_y$ as $|s| \to \infty$, possible contours of integration are given by Fig. 15. The

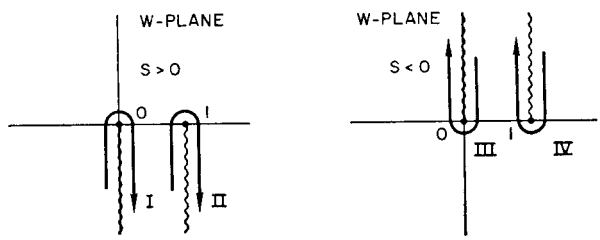


FIG. 15.—Integration contours for the extraordinary wave, normal incidence.

major contribution to $E_y$ for $|s| \to \infty$ comes from the region $\mathrm{Im} w \approx 0$. The asymptotic behaviour of $E_I$, for example, can be calculated by substituting $w = e^{-i\pi/2} z/2s$, $w - 1 \approx e^{i\pi}$, where $z$ is a real integration variable and the phases of $w$, $w - 1$ are determined by the cut structure in Fig. 15. Carrying out the integration gives

$$E_{\mathrm{I}}(s) \to \frac{iA}{2} e^{is}(2s)^{is_0/2} e^{\pi s_0/4}(1 - e^{-\pi s_0})\Gamma(1 - \tfrac{1}{2}is_0). \tag{48}$$

Similarly one finds

$$E_{\mathrm{II}}(s) \to -\frac{iA}{2} e^{-is}(2s)^{-is_0/2} e^{\pi s_0/4}(1 - e^{-\pi s_0})\Gamma(1 + \tfrac{1}{2}is_0) \tag{49}$$

and for $s < 0$,

$$\begin{aligned} E_{\mathrm{III}}(s) &\to \frac{iA}{2} e^{is}(-2s)^{is_0/2} e^{-\pi s_0/4}(e^{\pi s_0} - 1)\Gamma(1 - \tfrac{1}{2}is_0) \\ E_{\mathrm{IV}}(s) &\to -\frac{iA}{2} e^{-is}(-2s)^{is_0/2} e^{-\pi s_0/4}(e^{\pi s_0} - 1)\Gamma(1 + \tfrac{1}{2}is_0). \end{aligned} \tag{50}$$

$E_{\mathrm{I}}$ and $E_{\mathrm{III}}$ are thus right moving waves, and $E_{\mathrm{II}}$ and $E_{\mathrm{IV}}$ left moving. There is also one contour in the finite plane encircling both branch points which gives a solution. However, a second independent finite-plane contour does not exist, and this representation is therefore not useful.

For boundary conditions we choose $E_{\mathrm{I}}(s)$ i.e. a transmitted right-moving wave, for $s > 0$. Thus, for $s > 0$ we have the contour I. To continue analytically to $s < 0$, we are restricted to the lower half plane in $s$. (This can be shown necessary by including a small dissipative term in the problem.) Thus we must rotate the contour counterclockwise as $s$ is rotated clockwise. The contour I is successively distorted as

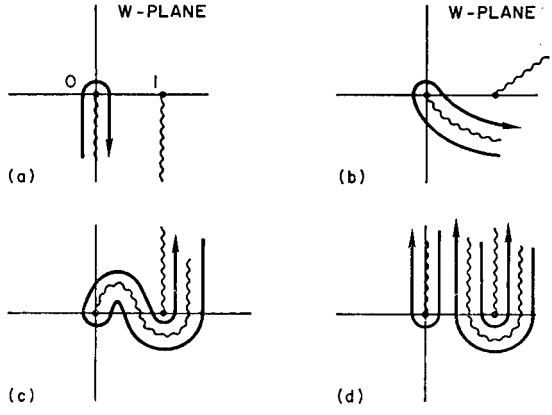


FIG. 16.—Distortion of the contour I for analytic continuation from $s > 0$ to $s < 0$.

shown in Fig. 16. From Fig. 16(d) it is seen that $E_{\mathrm{I}}$ becomes, after continuation to $s < 0$,

$$E_{\mathrm{I}} \to E_{\mathrm{IV}}(1 - e^{-\pi s_0}) + E_{\mathrm{III}}, \tag{51}$$

the two terms on the right representing the reflected and incident waves, respectively.

The transmission coefficient is given by equations (48) and (50):

$$|T| = |E_{\mathrm{I}}/E_{\mathrm{III}}| = e^{-\pi s_0/2}. \tag{52}$$

The reflection coefficient is the ratio of the two terms on the right-hand side of equation (51). From equation (50) we have

$$|R| = 1 - e^{-\pi s_0} \tag{53}$$

$|T|$ and $|R|$ are the same values given by BUDDEN (1961*c*), and their squares add up to less than unity. The deficit is the energy absorbed by the plasma at the hybrid resonance. In practice, the energy absorption may occur through mechanisms such as collisions with particles, collisions with turbulent fields, or generation of Bernstein waves. The rate of energy absorption, as shown explicitly in Section 3, is correctly given by the residues at the first-order poles of $\varepsilon(x)$, in spite of the fact that the dissipative mechanism has not been specified. This is because only the asymptotic behaviour of the fields is needed to calculate the energy loss, and the fluid equations are valid far from resonance. Inclusion of the dissipation mechanism will allow one to calculate the field amplitude near resonance, where the collisionless fluid equations break down, but the energy absorption there is already determined; and the amplitude must be such as to yield the correct energy loss. It is not necessary to assume, as Budden does, that energy flows away in the $z$ direction as the wave approaches resonance.

To calculate the field $E_{\mathrm{I}}$ near $s = 0$, we distort the contour of Fig. 15(a) into that shown in Fig. 17, which has three parts. It can easily be shown that the contribution

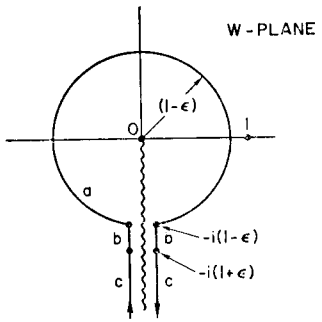


FIG. 17.—Integration contour for $s \approx 0$.

of part **b** of the contour is bounded by $\varepsilon s M$, where $M$ is a fixed number. The circular part **a** yields a contribution bounded by $sN$, with $N$ a fixed number. Part **c** of the contour yields, for $\varepsilon \to 0$,

$$E_{\mathrm{I}}(0) = -\frac{iA}{2}(e^{-\pi s_0} - 1). \tag{54}$$

Thus, $E_y$ is finite at the resonance. Dividing by the normalization of the incoming wave $E_{\mathrm{III}}$ (equation 50) we find

$$|E_y(0)| = Ae^{-3\pi s_0/4}/|\Gamma(1 - \tfrac{1}{2}is_0)|. \tag{55}$$

equation (11) then gives $E_x(s)$, which becomes infinite at $s = 0$ in the absence of collisions. For finite $\nu \ll \omega$ equations (39) and (11) become

$$\frac{k^2(s)}{k_0^2} = 1 - \frac{\omega_p^2}{\omega^2} \frac{\omega^2 - \omega_p^2 + i\nu\omega}{\omega^2 - \omega_h^2 + i\frac{\nu}{\omega}(2\omega^2 - \omega_p^2)} \tag{56}$$

$$\frac{iE_x}{E_y} = \frac{\omega_c}{\omega} \frac{\omega_p^2}{\omega^2 - \omega_h^2 + i\frac{\nu}{\omega}(2\omega^2 - \omega_p^2)} . \tag{57}$$

The collision frequency produces an insignificant change in $E_y$ but determines the amplitude of $E_x(0)$. Substituting the expression for $E_y(0)$ obtained above we then find

$$|E_x(0)| = \frac{\omega_c}{\omega} \frac{\omega^2 - \omega_c^2}{\omega^2 + \omega_c^2} \frac{\omega}{\nu} \frac{Ae^{-3\pi s_0/4}}{|\Gamma(1 - \frac{1}{2}is_0)|} . \tag{58}$$

Figures 18 and 19 show the spatial behaviour of $|E|^2$ for two values of $k_0x_0$, as computed by direct integration of equation (47) using the appropriate contour

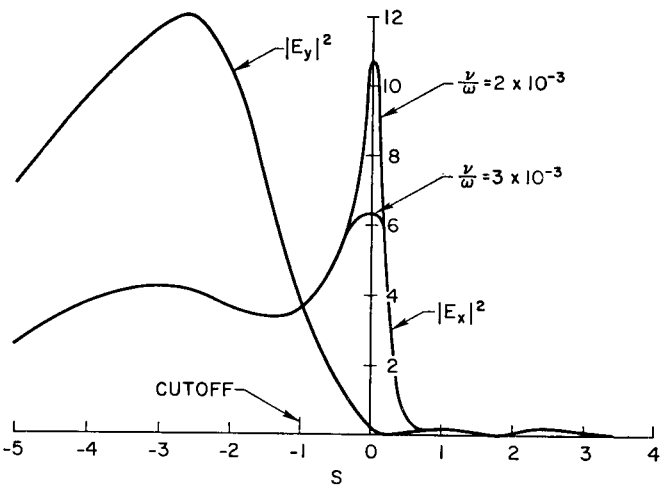


FIG. 18.—Computed wave intensity profiles for the Budden problem for $k_0x_0 = 1$ and two values of the collision frequency $\nu$. The incoming wave has amplitude $|E_y|^2 = 1$.

in Fig. 15. A moderately large collision rate, $\nu/\omega = 2 \times 10^{-3}$, is sufficient to make the field peaking near hybrid resonance unimportant. A value of $\omega_c/\omega = 6 \times 10^{-2}$ was used to calculate $E_x$. In the experiments of WONG *et al.* (1970), however, the density was sufficiently low ($n = 10^9$ cm$^{-3}$, $\nu/\omega = 1{\cdot}3 \times 10^{-5}$) that the coupling to ion oscillations could have been caused by the steep field gradient near resonance.

### 2.4 *The extraordinary wave at oblique incidence*

When the plasma radius is large compared to the wavelength, the upper hybrid resonance is inaccessible; and the wave amplification in the geometry of Budden's

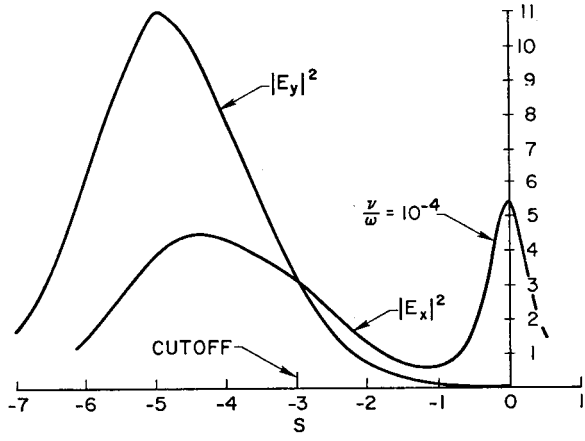


FIG. 19.—Same as Fig. 18, for $k_0x_0 = 3$.

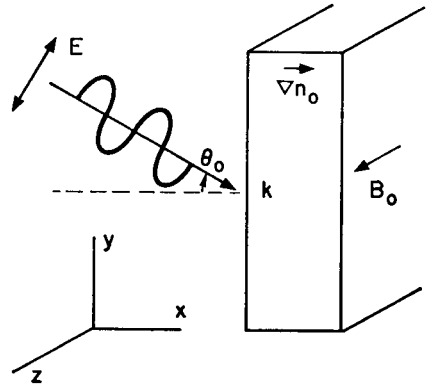


FIG. 20.—Geometry for the extraordinary wave at oblique incidence.

problem is not practical. One then asks whether the TM mode at oblique incidence has an accessible resonance. The answer is unfortunately no.

When $\mathbf{B}_0$ is large, this mode is an extraordinary wave and is governed by equations (12) and (13) with the $\omega_c$ terms retained. The geometry is shown in Fig. 20. Eliminating $E_x$ between equations (12) and (13) and simplifying, one obtains the following equation for $E_y$:

$$\frac{d^2E_y}{ds^2} + p(s)\frac{dE_y}{ds} + q(s)E_y = 0, \qquad s \equiv k_0x \tag{59}$$

where

$$p(s) = \frac{d}{ds}(\omega_p^2)\frac{\sin^2\theta_0}{(\omega^2 - \omega_h^2)\left(\cos^2\theta_0 - \dfrac{\omega_p^2}{\omega^2 - \omega_c^2}\right)} \tag{60}$$

$$q(s) = 1 - \frac{\omega_p^2}{\omega^2}\frac{\omega^2 - \omega_p^2}{\omega^2 - \omega_h^2} - \sin^2\theta_0 - \frac{d}{ds}(\omega_p^2)\frac{\omega_c}{\omega}\frac{\sin\theta_0\cos^2\theta_0}{(\omega^2 - \omega_h^2)\cos^2\theta_0 - \dfrac{\omega_p^2}{\omega^2 - \omega_c^2}} \tag{61}$$

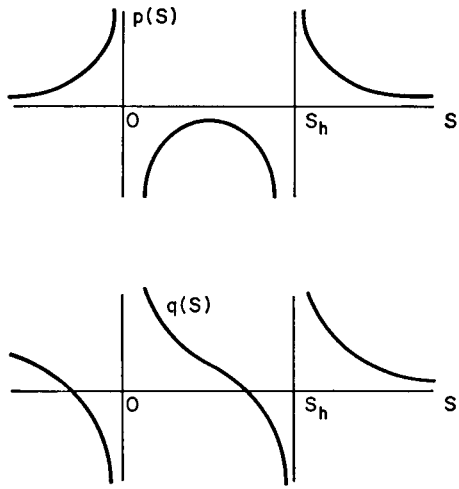


FIG. 21.—Schematic behavior of the coefficients $p(s)$, $q(s)$.

We have made the low-$\beta$ assumption that $\omega_c$ is uniform; the entire $s$ dependence then occurs in $\omega_p^2(s)$. The characteristic behaviour of $p(s)$ and $q(s)$ for a monotonically increasing density profile is shown in Fig. 21. We have for convenience defined the origin ($s = 0$) to be at the point where $(\omega_p^2)/(\omega^2 - \omega_c^2) = \cos^2\theta_0$. Both $p$ and $q$ have first order singularities at this point, as well as at $s_h$, where $\omega^2 = \omega_h^2$. Further, $p(s)$ is identically zero at the plasma boundary, whereas $q(s)$ is asymptotically equal to $\cos^2\theta_0$. Their Laurent expansions about $s = 0$ are given by

$$\begin{aligned} p(s) &= -\frac{1}{s} + \dots \\ q(s) &= \frac{\omega_c}{\omega}\frac{\cos^2\theta_0}{s\sin\theta_0} + \dots \end{aligned} \tag{62}$$

Introduce the transformation $E_y(s) = U(s)h(s)$ with

$$h(s) = \exp\left(-\int_{-\infty}^{s} \tfrac{1}{2}p(s')\,ds'\right). \tag{63}$$

Then $U(s)$ satisfies the equation

$$\frac{d^2U}{ds^2} + k^2(s)U(s) = 0$$

with

$$k^2(s) = q(s) - \tfrac{1}{2}p'(s) - \tfrac{1}{4}p^2(s). \tag{64}$$

The structure of $k^2(s)$ is easily seen to consist of a cutoff, two second order singularities at $s = 0$ and $s = s_h$, and first order singularities at the same points. It is clear from equation (62) that the coefficients of the second order poles are independent of the details of the plasma density profile. Also, $\lim_{s\to-\infty} k^2(s) = \cos^2\theta_0$.

Figure 22 shows $k^2(s)$ for the density profile $\omega_p^2/\omega^2 = (1 + \tanh s)/2$ for various

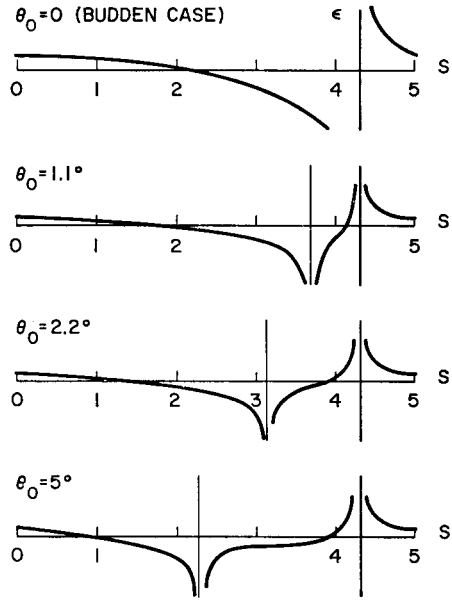


FIG. 22.—Behaviour of the effective dielectric constant $k^2(s)$ for the extraordinary wave at varying angles of incidence. The curves were computed for $\omega_c^2/\omega^2 = 2 \times 10^{-4}$ and $\omega_p^2(s)/\omega^2 = \frac{1}{2}(1 + \tanh s)$.

values of $\theta_0$. As $\theta_0 \to 0$ the second order poles merge and cancel, $p(s) \to 0$, and the problem reduces to the one treated in Section 2.3, Fig. 13. The point $s = 0$ is a regular singular point of equation (59). From the collisional counterpart of equation (12) one obtains

$$E_x(s) = i \frac{\dfrac{\omega_c}{\omega} \dfrac{\omega_p^2}{(\omega + i\nu)^2 - \omega_c^2} E_y(s) - \sin\theta_0 E_y'(s)}{\dfrac{\omega_p^2(1 + i\nu/\omega)}{(\omega + i\nu)^2 - \omega_c^2} - \cos^2\theta_0}, \tag{65}$$

which shows an apparent resonance behaviour at $s = 0$. In fact one can show using the expansions of $p(s)$, $q(s)$ near $s = 0$ together with equation (12), (13) that the numerator in the r.h.s. of equation (65) vanishes at $s = 0$ and $E_x(0)$ is finite. There is a resonance at $s = s_h$ at which $E_x = \infty$ in the absence of collisions. Figure 22 shows the dependence of the distance between resonance and cutoff on incident angle $\theta_0$. The physical reasons for the cutoff and resonance are as follows. At $s = s_h$, the wave has the usual hybrid resonance because the wavelength is infinitely short, so that the plasma inhomogeneity is negligible. Thus, the square of the frequency, $\omega^2 = \omega_p^2 + \omega_c^2$, is determined equally by the electrostatic restoring force ($\omega_p^2$ term) and the Lorentz force ($\omega_c^2$ term). The cutoff occurring to the left of this resonance is the usual right-hand cutoff modified by finite $\theta_0$. In the limit of weak density gradient and far from resonance, we have $p(s) \approx 0, q(s) \approx \varepsilon_x - \sin^2\theta_0$, in analogy with equation (24) and (27). The physical explanation is the same as for the ordinary wave, since $\varepsilon_x$ is isotropic as long as $\mathbf{k}$ is confined to the $x$–$y$ plane. Cutoff then occurs at

$$\frac{\omega_p^2}{\omega^2} \approx 1 \mp \frac{\omega_c}{\omega} \cos\theta_0. \tag{66}$$

## 3. LINEAR (RESONANCE) ABSORPTION

The phenomenon of linear or resonance absorption can be an important mechanism for the thermalization of electromagnetic energy in many cases of interest. It can in some cases be responsible for the thermalization of as much as half of the radiation incident on a plasma, and as the process has no threshold it is important also for low amplitude incident radiation. The process is due to poles in the dielectric constant which gives rise to a non-Hermitian Hamiltonian for the system, and the absorption of energy at a point in space with an associated non-unitarity of the $S$-matrix for the scattering process. This non-unitarity is generally the result of the vanishing of a particular channel in an idealized limit; e.g. the fluid limit. Although the modes of this channel do not exist in the idealized limit, the energy flux into these modes can be correctly given by the residue of the resulting singularity. As an illustration we calculate the energy absorption for the Budden problem and show that it is prescribed by the first-order poles of the dielectric function $\varepsilon$.

The Poynting vector is given by $x$

$$\mathbf{P} = \frac{c}{4\pi} \operatorname{Re}(\mathbf{E}e^{-i\omega t}) \times \operatorname{Re}\left(-\frac{ic}{\omega}\nabla \times \mathbf{E}e^{-i\omega t}\right). \tag{67}$$

We are interested in the $x$-component of $\mathbf{P}$, averaged over one cycle, which is

$$\bar{P}_x = \frac{ic^2}{16\pi\omega}\left(E_y\frac{\partial E_y^*}{\partial x} + E_z\frac{\partial E_z^*}{\partial x} - E_y\frac{\partial E_x^*}{\partial y} - E_z\frac{\partial E_x^*}{\partial z} - \text{c.c.}\right). \tag{68}$$

Then since $\mathbf{E}$ is independent of $y$ and $z$ we have

$$\bar{P}_x = \frac{ic^2}{16\pi\omega}\left(E_y\frac{\partial E_y^*}{\partial x} - \text{c.c.}\right). \tag{69}$$

Thus the divergence of $\bar{P}$ is given by

$$\frac{\partial \bar{P}_x}{\partial x} = -\frac{ic^2}{16\pi\omega}\left(E_y^*\frac{\partial^2 E_y}{\partial x^2} - \text{c.c.}\right) \tag{70}$$

or, from equation (46),

$$\frac{\partial \bar{P}_x}{\partial x} = \frac{ic^2k_0^2}{16\pi\omega}\left[\left(1 + \frac{x_0}{x}\right)E_y^*E_y - \text{c.c.}\right].$$

In the limit $\nu/\omega \to 0$,

$$\varepsilon_x = \varepsilon_x^h + x_0 i\pi\,\delta(x). \tag{71}$$

The Hermitian part $\varepsilon_x^h$ clearly does not contribute to energy loss from the wave; thus the relevant part of $\partial\bar{P}_x/\partial x$ is

$$\frac{\partial \bar{P}_x}{\partial x} = \frac{ic^2k_0^2}{16\pi\omega}|E_y|^2\,2\pi i x_0\,\delta(x), \tag{72}$$

and the absorbed energy is

$$-\Delta\bar{P}_x = \frac{c^2k_0^2x_0}{8\omega}|E_y(0)|^2. \tag{73}$$

Substituting the value of $E_y(0)$ from equation (55), we find

$$-\Delta\bar{P}_x = \frac{cs_0}{8}\frac{A^2 e^{-3\pi s_0/2}}{|\Gamma(1 - is_0/2)|^2}.$$

Using $\Gamma(-is_0/2) = -i(s_0/2)\Gamma(-is_0/2)$, $\Gamma^*(1 - is_0/2) = \Gamma(1 + is_0/2)$ and $\Gamma(z)\Gamma(1 - z) = \pi/\sin \pi z$, we find

$$-\Delta\bar{P}_x = \frac{cA^2}{8\pi}(e^{-\pi s_0} - e^{-2\pi s_0}). \tag{74}$$

Substituting the asymptotic forms of $E_y$ into equation (69), we find the total incoming and outgoing fluxes to be

$$\begin{aligned}\bar{P}_{\text{in}} &= \frac{cA^2}{8\pi}(1 - |R|^2)\\ \bar{P}_{\text{out}} &= \frac{cA^2}{8\pi}|T|^2.\end{aligned} \tag{75}$$

Substituting $|T|$ and $|R|$ from equations (52) and (53), we find

$$\bar{P}_{\text{in}} = \bar{P}_{\text{out}} - \Delta\bar{P};$$

and thus the resonant absorption due to the singularity in $\varepsilon$ accounts for the discrepancy in $|R|^2 + |T|^2 \neq 1$.

The absorption coefficient $e^{-\pi s_0} - e^{-2\pi s_0}$ is shown in Fig. 23 as a function of the tunneling distance $s_0$.

The absorption due to singularities in dielectric constants describing other processes can be calculated in a similar manner, but has been done only in a few cases

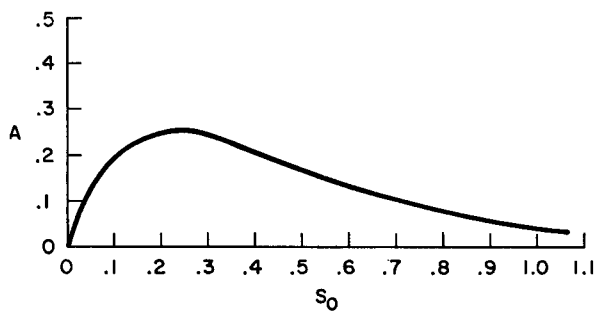


FIG. 23.—Absorption coefficient for linear absorption for the Budden problem.

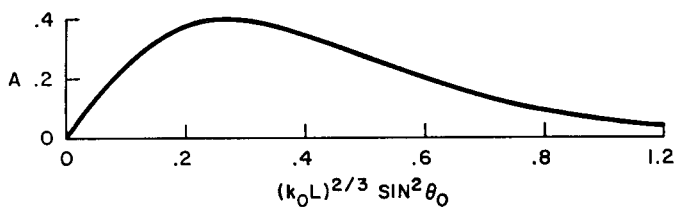


FIG. 24.—Absorption coefficient for linear absortion for an obliquely incident TM mode.

which readily admit analytic solution. In particular the problem of Section 2.2(c), an obliquely incident TM mode, has been analyzed extensively by PILIYA (1966) and more recently by FREIDBERG *et al.* (1972). The absorption in this case is a function of the single parameter $q = (k_0 L)^{2/3} \sin^2 \theta_0$ where $\theta_0$ is the angle of incidence, $k_0$ the free space wave number, and $L$ the density scale length. The absorption coefficient is shown in Fig. 24.

## 4. SUMMARY

We have considered the amplification of electromagnetic waves propagating into an inhomogeneous plasma at either normal or oblique incidence, both with and without an external magnetic field. Numerical results for the wave amplitude variation and energy absorption have been obtained for cases where such results cannot be found in the existing literature. An integral representation is given from which the amplification and absorption for all cases can be computed by direct integration. It is shown that the absorption is correctly given by the poles of the dielectric constant without collisions.

Enhancement of the wave intensity at a plasma cutoff depends only weakly on $k_0\Lambda$ and cannot ordinarily be made larger than about an order of magnitude. On the other hand, enhancement at an infinity of the effective dielectric constant (resonance) can be larger than $10^2$. The extraordinary wave at normal incidence exhibits this effect, but the resonance is not accessible if $k_0\Lambda$ is large. The ordinary wave at oblique incidence has a resonance which can always be made accessible by adjusting the angle of incidence. The angular range, however, becomes extremely small for large $k_0\Lambda$. In a strong magnetic field, the extraordinary wave at oblique incidence has an effective dielectric constant with two resonances. The wave amplitude, however, is resonant only at the upper hybrid point, which cannot be made accessible by adjusting the angle of incidence. A sufficiently large magnetic field, therefore, removes the resonant absorption associated with the TM mode at finite $\theta_0$. The computation of absorption in the general case is straightforward but tedious. For most purposes a sufficiently good approximation can be obtained by averaging the values given by Figs. 23 and 24.

*Acknowledgement*—One of the authors (RBW) would like to acknowledge the hospitality of the UCLA Plasma Physics Group, where this work was completed. Contour integrations were performed on the UCLA On-Line facility.

## REFERENCES

BAÑOS A., JR. (1972) UCLA Report PPG-124.

BAÑOS A., JR. and KELLY D. (1972) UCLA Report PPG-125.

BERK H. L. PEARLSTEIN L. D. (1972) University of California Radiation Laboratory Report UCRL 72536.

BREKHOVSKIKH L. M. (L960) *Waves in Layered Media*, p. 189. Academic Press, New York.

BUDDEN K. G. (1961*a*) *Radio Waves in the Ionosphere*, p. 319. Cambridge University Press, London.

BUDDEN K. G. (1961*b*) *Radio Waves in the Ionosphere*, Chapter 17. Cambridge University Press, London.

BUDDEN K. G. (1961*c*) *Radio Waves in the Ionosphere*, p. 476. Cambridge University Press, London.

DENISOV N. G. (1957) *Soviet Phys. JETP* **4**, 544.

FREIDBERG J. P., MITCHELL R. W., MORSE R. L. and RUDSINSKI L. I. (1972) *Phys. Rev. Lett.* **28**, 795.

GINZBURG V. L. (1964*a*) *Propagation of Electromagnetic Waves in Plasmas*, pp. 192–220. Pergamon Press, New York.

GINZBURG V. L. (1964*b*) *Propagation of Electromagnetic Waves in Plasmas*, pp. 364–368. Pergamon Press, New York.

HEALD M. A. and WHARTON C. B. (1965) *Plasma Diagnostics with Microwaves*, p. 83. Wiley, New York.
HORA H. (1969) *Phys. Fluids* **12**, 182.
LINDL J. D. and KAW P. K. (1971) *Phys. Fluids* **14**, 371.
PEARLSTEIN L. D. and BHADRA D. (1969) *Phys. Fluids* **12**, 213.
PILIYA A. D. (1966) *Soviet Phys. Tech. Phys.* **11**, 609.
WEYL G. M. (1970) *Phys. Rev. Lett.* **25**, 1417.
WHITTAKER E. T. and WATSON G. N. (1952) *Modern Analysis*, 4th ed. p. 340. Cambridge University Press, London.
WONG A. Y., BAKER D. R. and BOOTH N. (1970) *Phys. Rev. Lett.* **24**, 804.
WONG A. Y. and TAYLOR R. J. (1971) *Phys. Rev. Lett.* **27**, 644.
WONG A. Y., CHEN F. F., BOOTH N., JASSBY D. L., STENZEL R., BAKER D. and LIU C. S. (1971) *Plasma Physics and Controlled Nuclear Fusion Research*, Vol. 1, p. 335. IAEA, Vienna.